Brief communication: PICOP, a new ocean melt parameterization under ice shelves combining PICO and a plume model

Tyler Pelle[1], Mathieu Morlighem[1], and Johannes H. Bondzio[1]

[1]University of California, Irvine, Department of Earth System Science, Irvine, CA 92697-3100, USA

Correspondence: Tyler Pelle (tpelle@uci.edu)

Abstract. Basal melt at the bottom of Antarctic ice shelves is a major control on glacier dynamics, as it modulates the amount of buttressing that floating ice shelves exert onto the ice streams feeding them. Three-dimensional ocean circulation numerical models provide reliable estimates of basal melt rates but remain too computationally expensive for century scale projections. Ice sheet modelers therefore routinely rely on simplified parameterizations either based on ice shelf depth or on more sophisticated
5   box models. However, existing parameterizations do not accurately resolve the complex spatial patterns of sub-shelf melt rates that have been observed over Antarctica's ice shelves, especially in the vicinity of the grounding line, where basal melt is one of the primary drivers of grounding line migration. In this study, we couple the Potsdam Ice-shelf Cavity mOdel (PICO) to a buoyant Plume melt rate parameterization to create PICOP, a novel basal melt rate parameterization that is easy to implement in transient ice sheet numerical models and produces a melt rate field that is in excellent agreement with the spatial distribution and
10   magnitude of observations for a wide variety of ocean basins. We test PICOP on the Amundsen Sea sector of West Antarctica, Totten and Moscow University ice shelves in Eastern Antarctica, and the Ronne-Filchner ice shelf and compare the results to PICO. We find that PICOP is able to reproduce the high melt rates near the grounding lines of Pine Island, Thwaites, and Totten glaciers (on the order of 100 m/yr) and removes the "banding" pattern observed in melt rates produced by PICO over the Ronne-Filchner ice shelf. PICOP resolves many of the issues contemporary basal melt rate parameterizations face and is
15   therefore a valuable tool for those looking to make future projections of Antarctic glaciers.

1 Introduction

Glaciers around the periphery of the Antarctic Ice Sheet (AIS) have undergone dynamic changes due to the upwelling of warm modified Circumpolar Deep Water (mCDW) into sub-ice shelf cavities (e.g., Jacobs et al., 2011; Pritchard et al., 2012).
20   This process drives enhanced basal melt, which has the potential to reduce the buttressing effect that ice shelves exert on grounded ice upstream (e.g., Rignot and Jacobs, 2002). As this upwelling is expected to increase along sectors of the periphery the AIS due to the poleward intensification of the Southern Hemisphere westerly winds (Dinniman et al., 2012), accurately parameterizing these basal melt rates is necessary in making future projections of the AIS due to the large computational cost

of two way ice-ocean model coupling. Many early basal melt parameterizations (i.e., parameterizations based on the local heat flux at the ice-ocean interface (DeConto and Pollard, 2016; Beckmann and Goosse, 2003) or on basal slopes (Little et al., 2012)) do not accurately capture the impact of ocean circulation within sub-shelf cavities, which is a key control of basal melting. Two of the most recently published melt parameterizations that resolve sub-shelf ocean circulation are the Potsdam

5 Ice-shelf Cavity mOdel (PICO, Reese et al., 2018) and one based on the physics of buoyant meltwater plumes (Plume model, Lazeroms et al., 2018). Although both parameterizations are novel in their own regards, melt rates calculated by PICO suffer from unrealistic "banding" as a product of its box model approach and remain too low near grounding lines. In addition, the Plume model requires complete sub-shelf ocean temperature and salinity fields as inputs, and has not been adapted to use in transient model runs. We overcome these limitations by combining both PICO and the Plume model to form PICOP: we rely on

10 PICO's box model to reconstruct the temperature and salinity fields beneath ice shelves based on far field ocean properties and then use this reconstruction to drive the Plume model, which calculates the basal melt rate field. In this brief communication, we describe the physics used to derive PICOP and compare melt rates produced by PICO and PICOP to observations by Rignot et al. (2013) in three basins of varying oceanic conditions and geometry.

2 Methods

15 ## 2.1 PICO

PICO is a two-dimensional sub-shelf melt rate parameterization that was designed to reproduce the density driven overturning circulation within sub-shelf cavities and is used here to produce ambient ocean temperature and salinity fields (Reese et al., 2018). Inputs for PICO are the basin-averaged ocean temperature T and salinity S and sub-shelf ocean circulation is driven by the *ice pump* mechanism (Lewis and Perkin, 1986). Individual mesh elements or grid cells within the model domain are

20 assigned a box number based on their relative distance from both the grounding line and ice front. In general, PICO solves for the transport of heat and salt between boxes in contact with the base of the ice shelf, starting at the grounding line and ending at the ice front (boxes B_k for k = $\{1, \ldots, n\}$, where n is typically less than or equal to 5). After simplification and assuming steady state conditions, the balance of heat and salt in all boxes along the base of the ice shelf can be written as:

$$
\begin{aligned}
q \left(T_{k-1} - T_k\right) - A_k m_k \frac{\rho_i}{\rho_w} \frac{L}{c_p} &= 0 \\
q \left(S_{k-1} - S_k\right) - A_k m_k S_k &= 0.
\end{aligned}
\tag{1}
$$

25 Using a simplified formulation of the 3-equation melt model by Holland and Jenkins (1999), the transport equations can be solved for salinity S_k and temperature T_k in box B_k, and are dependent on the local pressure p_k, the box area A_k, and the temperature T_{k-1} and salinity S_{k-1} of the upstream box B_{k-1}. The strength of the overturning circulation, q, is calculated once per time-step in box B_1 from the density difference between the far field and grounding line water masses:

$$
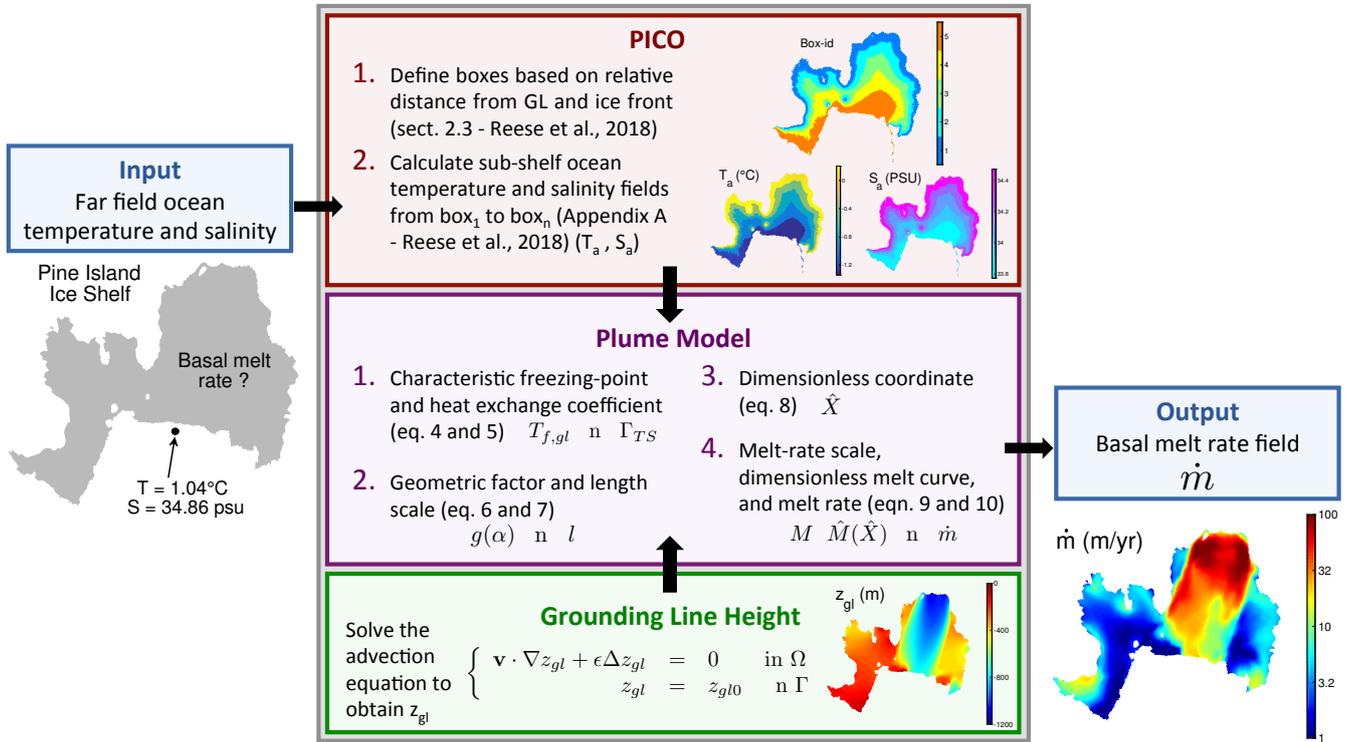q = C(\rho_0 - \rho_1).
\tag{2}
$$

Figure 1. Schematic diagram of PICOP with example data displayed for the Pine Island ice shelf of West Antarctica. The inputs into the parameterization are the basin averaged ocean temperature (°C) and salinity (psu), which are first fed into PICO (red box). PICO uses these inputs to calculate the sub-shelf ambient ocean temperature and salinity fields, which are then used in the Plume model (purple box). In addition, the grounding line height is calculated at this time by solving the advection problem defined in the green box. Once these three fields are fed into the Plume model, the basal melt rate field is computed according to the steps outlined in the purple box.

Here, we do not use PICO's melt rate parameterization but only use the sub-shelf temperature and salinity fields to drive the Plume model (Fig. 1). All constants and external parameters referenced in this paper are summarized in Table 1. For a full derivation of PICO, see Reese et al. (2018).

2.2 Plume model

The Plume model is a basal melt rate parameterization based on the theory of buoyant melt water plumes that travel upward along the base of the ice shelf from the grounding line to the location where the plume loses buoyancy. The two-dimensional formulation from Lazeroms et al. (2018) is adapted from the one-dimensional plume model developed by Jenkins (1991) for a plume traveling in direction X with temperature T, and salinity S in an ocean with ambient temperature T_a and salinity S_a (provided by PICO). We begin by defining the grounding line depth, z_{gl}, over the entire ice shelf, as it is necessary to determine where individual plumes originate in order to employ this parameterization. As a first approximation, we solve an advection

equation:

$$\begin{cases} \mathbf{v} \cdot \nabla z_{gl} + \epsilon \Delta z_{gl} &=& 0 & \text{in } \Omega \\ z_{gl} &=& z_{gl0} & \text{on } \Gamma \end{cases} \tag{3}$$

where z_{gl0} is the grounding line depth defined at the grounding line Γ, Ω is the ice shelf, and as a first approximation, $\mathbf{v}$ is the ice depth-averaged velocity. Note that ϵ is a small diffusion coefficient introduced to minimize noise and to provide numerical
5 stability. We therefore make the assumption that melt water plumes coincide with ice velocities. We attempted using other advection schemes, for example based on basal slopes, but the level of noise made these approaches unpractical.

In a second step, we correct z_{gl} such that, if z_{gl} is greater than the height of the base of the ice shelf, z_b, then we set $z_{gl} = z_b$. Compared to the algorithm used to determine z_{gl} in Lazeroms et al. (2018), advecting grounding line heights is computationally more efficient for higher resolution model runs because we do not have to search for multiple possible plume sources at every
10 point within a given ice shelf.

Now that z_{gl} is defined, we continue by computing both the characteristic freezing point $T_{f,gl}$ and the effective heat exchange coefficient Γ_{TS} as follows:

$$T_{f,gl} = \lambda_1 S_a + \lambda_2 + \lambda_3 z_{gl} \tag{4}$$

$$\Gamma_{TS} = \Gamma_T \left(\gamma_1 + \gamma_2 \frac{T_a - T_{f,gl}}{\lambda_3} \times \frac{E_0 \sin \alpha}{C_d^{1/2} \Gamma_{TS_0} + E_0 \sin \alpha} \right). \tag{5}$$

15 A geometric scaling factor $g(\alpha)$ and length scale l are defined in order to give the plume model the proper geometry dependence and scaling according to the distance traveled along the plume path. The scaling factor and length scale are computed as follows:

$$g(\alpha) = \left(\frac{\sin \alpha}{C_d + E_0 \sin \alpha} \right)^{1/2} \left(\frac{E_0 \sin \alpha}{C_d^{1/2} \Gamma_{TS} + E_0 \sin \alpha} \right)^{1/2} \left(\frac{E_0 \sin \alpha}{C_d^{1/2} \Gamma_{TS} + E_0 \sin \alpha} \right) \tag{6}$$

$$l = \frac{T_a - T_{f,gl}}{\lambda_3} \times \frac{x_0 C_d^{1/2} \Gamma_{TS} + E_0 \sin \alpha}{x_0 \left(C_d^{1/2} \Gamma_{TS} + E_0 \sin \alpha \right)}. \tag{7}$$

20 The dimensionless scale factor x_0 used in the second term of l defines the transition-point between melting and refreezing and is constant for all model results. For a complete explanation of the individual terms that make up these two factors, see section 2.2 of Lazeroms et al. (2018).

The length scale is then used in the computation of the dimensionless coordinate, $\hat{X}$:

$$\hat{X} = \frac{z_b - z_{gl}}{l}. \tag{8}$$

25 Note that $\hat{X} = 0$ corresponds to the position of the grounding line and $\hat{X} = 0.56$ is the aforementioned transition point, but $\hat{X} = 1$ does not necessarily correspond to the position of the calving front due to the dependence of $\hat{X}$ on l. In order to ensure valid values of $\hat{X}$, we set a lower bound for the ambient ocean temperature: $T_a \geq \lambda_1 S_a + \lambda_2$. The melt rate $\dot{m}$ is then calculated

as

$$\dot{m} = \hat{M}(\hat{X}) \times M, \tag{9}$$

where $\hat{M}(\hat{X})$ is a dimensionless melt curve defined in Lazeroms et al. (2018) and M is defined as

$$M = M_0 \times g(\alpha) \times \left(T_a - T_f(S_a, z_{gl})\right)^2. \tag{10}$$

5   For a full derivation of the buoyant plume model used in PICOP, see Lazeroms et al. (2018).

3   Results and Discussion

We evaluate PICOP using geometry from Bedmap2 (Fretwell et al., 2013) and far field ocean temperature and salinity values averaged at the depth of the continental shelf between 1975 to 2012 (Reese et al., 2018; Schmidtko et al., 2014). Here, we compare the modeled basal melt rates calculated by PICO and PICOP to melt rates inferred from conservation of mass and

10   satellite interferometry (Rignot et al., 2013), that we refer to as "observations". We focus on three regions: the Amundsen Sea sector of the West Antarctic Ice Sheet, the Totten and Moscow University ice shelves of the East Antarctic Ice Sheet, and the Ronne-Filchner ice shelf. Model inputs for these basins are (1.04°C, 34.86 psu), (-0.73°C, 34.73 psu), and (-1.76°C, 34.82 psu), respectively.

The spatial distribution of melt rates produced by PICOP is in significantly better agreement with observations compared

15   to PICO, especially in the vicinity of the grounding line where accurate melt rates are needed in order to correctly capture the glacier's grounding line dynamics. In Fig. 2, we see that modeled melt rates produced by PICOP reach approximately 100 m/yr near the grounding line of Pine Island and Thwaites glaciers as compared to approximately 40 m/yr by PICO. These high melt rates are a product of the deeply entrenched bed that both Pine Island and Thwaites glaciers are grounded to. These bed depths are advected with the ice velocity when z_{gl} is solved for, leading to high melt rates that better match observations.

20   A similar situation occurs under Totten ice shelf; melt rates modeled by PICOP reach a maximum of about 50 m/yr, while those from PICO reach a maximum of approximately 20 m/yr. Modeling these high melt rates is especially important in the upstream-most portion of Totten's grounding line, where complex grounding line retreat has been observed over the past 17 years and has been found to be strongly sensitive to changes in ocean temperature (Li et al., 2015). Over the Ronne-Filchner ice shelf, the inherent geometry dependence of PICOP reduced the "banding" that modeled melt rates from PICO displayed.

25   This is a significant improvement because as can be seen in Fig. 2, there is a very sharp gradient in the melt rate field computed by PICO over the Ronne-Filchner ice shelf that would lead to unrealistic ice-shelf dynamics in transient model runs. PICOP produces a smooth transition from high to low melt rates that better matches observations. Additionally, significant melt was computed near the ice front of this ice shelf, which is a product of the high slopes that PICOP considers when computing melt rates.

30   In all three basins, area-weighted mean melt rates calculated with PICOP show significantly better agreement with Rignot et al. (2013). The values reported in figure two corresponding to PICO differ from those used in figure 5 of Reese et al. (2018)
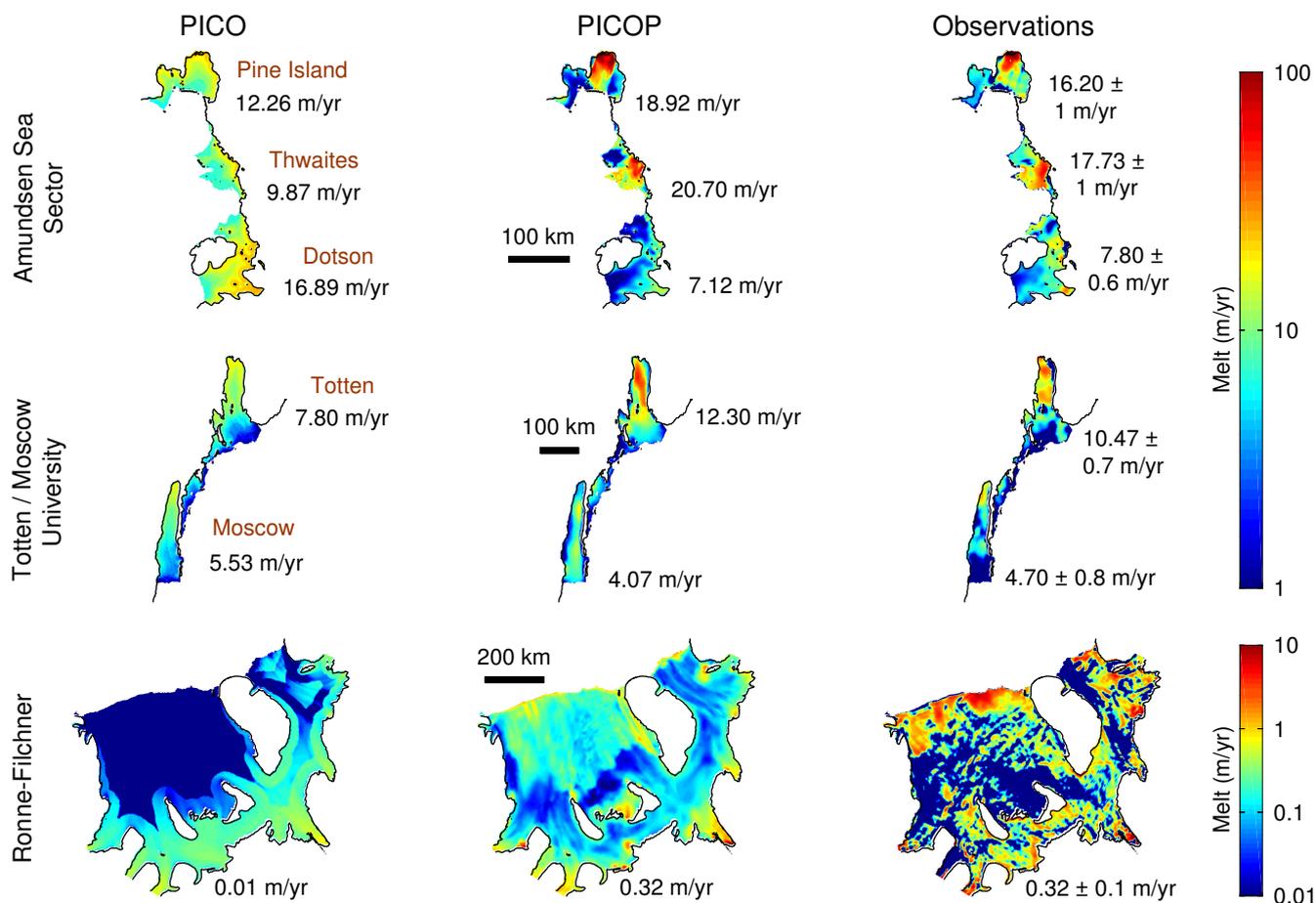
Figure 2. Modeled (PICO and PICOP) and observed (Rignot et al., 2013) melt rates (m/yr) are displayed for the Amundsen Sea sector of West Antarctica (including Pine Island, Thwaites, and Dotson ice shelves), Totten and Moscow University ice shelves of East Antarctica, and the Ronne-Filchner ice shelf. Numerical values under PICO and PICOP are area weighted mean melt rates. The observed annual mean melt rate is displayed under the observed melt rate panel.

because we model these basins using a significantly higher mesh resolution (minimum element size of 500 m, maximum of 10 km). By modeling Totten, Pine Island, and Thwaites ice shelves with a coarse mesh, only two boxes were defined for these smaller shelves in Reese et al. (2018), and thus, a larger proportion of the ice shelf was modeled as the grounding-line box. Melt rates computed in this box are the highest across the shelf because no heat has been lost from the ocean water by the

5   addition of cold melt water, leading to higher mean melt rates when compared to those displayed in figure 2. By using a finer mesh to evaluate PICOP, we are able to capture the fine details of the melt pattern, which are key in predicting the evolution of grounding line dynamics, as well as maintain shelf-averaged melt rates that are in relatively good agreement with observations. The mean melt rates of Pine Island, Thwaites, and Totten ice shelves are slightly overestimated (18.92 m/yr, 20.70 m/yr and 12.30 m/yr, respectively) when modeled with PICOP due to the strong grounding line advection used to compute z_{gl} in these

regions. Over the Ronne-Filchner ice shelf, PICOP models a shelf-mean melt rate that is in better agreement with observation than PICO does because PICOP produces melt further downstream of the grounding line as a result of its geometry dependence. In this sector of the ice shelf, PICO primarily computes refreezing ($\dot{m} < 0$), which drives the mean melt rate down to 0.01 m/yr.

While PICOP resolves many of the issues displayed in contemporary sub-shelf mate rate parameterizations, it is limited by

5 the assumptions that were made when both PICO and the Plume model were originally derived (see Reese et al. (2018) and Lazeroms et al. (2018)). In addition, when computing z_{gl}, we assume that melt water plumes travel in the same direction as the ice velocity rather than in the direction of the greatest basal slope. In doing so, we inevitably consider erroneous plume paths that lead to inconsistencies in the computed melt rate fields. Finally, PICOP does not model refreezing well in cold basins due to the lower limit imposed on the ambient ocean temperature. The ocean temperature output from PICO in cold basins

10 (i.e. the Ronne-Filchner and Ross ice shelves) falls below this lower bound, especially in the vicinity of the ice front, where the coldest ocean temperatures are modeled. As such, melt rates computed in the coldest cavities cannot be further improved unless this constraint is relaxed, as discussed in Appendix A of Lazeroms et al. (2018). Yet, PICOP remains an accurate and computationally efficient melt rate parameterization that can be easily implemented into high resolution, transient ice sheet numerical models.

15 **4 Conclusions**

Here, we presented a new basal melt rate parameterization that is a combination of both PICO and a Plume model. By utilizing PICO to resolve the sub-shelf ocean circulation and produce ambient ocean temperature and salinity fields, we reduce model inputs to only basin-averaged values. Additionally, the geometry dependence of the Plume model produces melt rates that show better agreement with observations in terms of both spatial distribution and magnitude than with PICO alone. As ocean

20 induced melting has been cited as a major driver of change for Antarctic glaciers and because Southern Ocean conditions are projected to change within the coming century, the improvements to the spatial distribution and magnitude of modeled melt rates produced by PICOP, as well as the computational efficiency of this parameterization, offer a valuable tool to more accurately make future projections of Antarctic glaciers.

Code and data availability. The data used in this study are freely available on the National Snow and Ice Data Center, or upon request to the

25 authors. ISSM is open source and freely available at http://issm.jpl.nasa.gov.

Author contributions. TP developed the idea of combining PICO and a plume model, and implemented it into ISSM with help from MM and JB. All authors participated in the writing of the manuscript.

Competing interests. None

Table 1. Constants and external quantities referenced in this communication. See Reese et al. (2018) and Lazeroms et al. (2018) for a full list of constants used to derive PICOP.

External Quantity	Symbol	Value	Unit
Far-field ocean temperature	T	-	°C
Far-field ocean salinity	S	-	PSU
Ambient ocean temperature	T_a	-	°C
Ambient ocean temperature	S_a	-	PSU
Local depth of ice shelf base	z_b	-	m
Local slope angle	α	-	-
Grounding line depth	z_{gl}	-	m
Basal melt rate	$\dot{m}$	-	m/yr

Constant Parameter	Symbol	Value	Unit
Gravitational acceleration	g	9.8	m s^{-2}
Density of ice	ρ_i	910	kg m^{-3}
Density of sea water	ρ_w	1028	kg m^{-3}
Latent heat of fusion	L	$3.34 \cdot 10^5$	J kg^{-1}
Heat capacity of sea water	c_p	3974	J kg^{-1} °C
Overturning strength	C	$1 \cdot 10^6$	m^6 s^{-1} kg^{-1}
Entrainment coefficient	E_0	$3.6 \cdot 10^{-2}$	-
Drag coefficient	C_d	$2.5 \cdot 10^{-3}$	-
Turbulent heat exchange coefficient	$C_d^{1/2}\Gamma_T$	$1.1 \cdot 10^{-3}$	-
Freezing point-salinity coefficient	λ_1	$-5.73 \cdot 10^{-2}$	°C
Freezing point offset	λ_2	$8.32 \cdot 10^{-2}$	°C
Freezing point-depth coefficient	λ_3	$7.61 \cdot 10^{-4}$	K m^{-1}
Melt-rate parameter	M_0	10	m yr^{-1} °C^{-2}
Heat exchange parameter	$C_d^{1/2}\Gamma_{TS_0}$	$6.0 \cdot 10^{-4}$	-
Heat exchange parameter	γ_1	0.545	-
Heat exchange parameter	γ_2	$3.5 \cdot 10^{-5}$	m^{-1}
Dimentionless scaling factor	x_0	0.56	-

References

Beckmann, A. and Goosse, H.: A parameterization of ice shelf–ocean interaction for climate models, Ocean Modelling, 5, 157–170, 2003.

DeConto, R. and Pollard, D.: Contribution of Antarctica to past and future sea-level rise, Nature, 531, 591–597, https://doi.org/10.1038/nature17145, 2016.

5   Dinniman, M., Klinck, J., and Hofmann, E.: Sensitivity of circumpolar deep water transport and ice shelf basal melt along the west Antarctic Peninsula to changes in the winds, J. Oceanogr., 25, 4799–4816, https://doi.org/10.1175/JCLI-D-11-00307.1, 2012.

Fretwell, P., Pritchard, H. D., Vaughan, D. G., Bamber, J. L., Barrand, N. E., Bell, R., Bianchi, C., Bingham, R. G., Blankenship, D. D., Casassa, G., Catania, G., Callens, D., Conway, H., Cook, A. J., Corr, H. F. J., Damaske, D., Damm, V., Ferraccioli, F., Forsberg, R., Fujita, S., Gim, Y., Gogineni, P., Griggs, J. A., Hindmarsh, R. C. A., Holmlund, P., Holt, J. W., Jacobel, R. W., Jenkins, A., Jokat, W., Jordan,

10   T., King, E. C., Kohler, J., Krabill, W., Riger-Kusk, M., Langley, K. A., Leitchenkov, G., Leuschen, C., Luyendyk, B. P., Matsuoka, K., Mouginot, J., Nitsche, F. O., Nogi, Y., Nost, O. A., Popov, S. V., Rignot, E., Rippin, D. M., Rivera, A., Roberts, J., Ross, N., Siegert, M. J., Smith, A. M., Steinhage, D., Studinger, M., Sun, B., Tinto, B. K., Welch, B. C., Wilson, D., Young, D. A., Xiangbin, C., and Zirizzotti, A.: Bedmap2: improved ice bed, surface and thickness datasets for Antarctica, Cryosphere, 7, 375–393, https://doi.org/10.5194/tc-7-375-2013, 2013.

15   Holland, D. and Jenkins, A.: Modeling thermodynamic ice-ocean interactions at the base of an ice shelf, J. Phys. Oceanogr., 29, 1787–1800, 1999.

Jacobs, S. S., Jenkins, A., Giulivi, C. F., and Dutrieux, P.: Stronger ocean circulation and increased melting under Pine Island Glacier ice shelf, Nat. Geosci., 4, 519–523, https://doi.org/10.1038/NGEO1188, 2011.

Jenkins, A.: A one-dimensional model of ice shelf-ocean interaction, J. Geophys. Res., 96, 20 671–20 677, 1991.

20   Lazeroms, W. M. J., Jenkins, A., Gudmundsson, G. H., and van de Wal, R. S. W.: Modelling present-day basal melt rates for Antarctic ice shelves using a parametrization of buoyant meltwater plumes, The Cryosphere, 12, 49–70, https://doi.org/10.5194/tc-12-49-2018, 2018.

Lewis, E. and Perkin, R.: Ice Pumps And Their Rates, J. Geophys. Res., 91, 1756–1762, 1986.

Li, X., Rignot, E., Morlighem, M., Mouginot, J., and Scheuchl, B.: Grounding line retreat of Totten Glacier, East Antarctica, 1996 to 2013, Geophys. Res. Lett., 42, 8049–8056, https://doi.org/10.1002/2015GL065701, 2015.

25   Little, C. M., Goldberg, D., Gnanadesikan, A., and Oppenheimer, M.: On the coupled response to ice-shelf basal melting, J. Glaciol., 58, https://doi.org/10.3189/2012JoG11J037, 2012.

Pritchard, H. D., Ligtenberg, S. R. M., Fricker, H. A., Vaughan, D. G., van den Broeke, M. R., and Padman, L.: Antarctic ice-sheet loss driven by basal melting of ice shelves, Nature, 484, 502–505, https://doi.org/10.1038/nature10968, 2012.

Reese, R., Albrecht, T., Mengel, M., Asay-Davis, X., and Winkelmann, R.: Antarctic sub-shelf melt rates via PICO, The Cryosphere, 12,

30   1969–1985, https://doi.org/10.5194/tc-12-1969-2018, 2018.

Rignot, E. and Jacobs, S.: Rapid bottom melting widespread near Antarctic ice sheet grounding lines, Science, 296, 2020–2023, https://doi.org/10.1126/science.1070942, 2002.

Rignot, E., Jacobs, S., Mouginot, J., and Scheuchl, B.: Ice shelf melting around Antarctica, Science, 341, 266–270, https://doi.org/10.1126/science.1235798, 2013.

35   Schmidtko, S., Heywood, K., Thompson, A., and Aoki, S.: Multidecadal warming of Antarctic waters, Science, 346, https://doi.org/10.1126/science.1256117, 2014.